Nanoscale Res Lett (2009) 4:1073–1077
DOI 10.1007/s11671-009-9360-4

NANO EXPRESS

Alloying and Strain Relaxation in SiGe Islands Grown on Pit-Patterned Si(001) Substrates Probed by Nanotomography

F. Pezzoli · M. Stoffel · T. Merdzhanova · A. Rastelli · O. G. Schmidt

Received: 30 April 2009 / Accepted: 24 May 2009 / Published online: 6 June 2009

Abstract The three-dimensional composition profiles of individual SiGe/Si(001) islands grown on planar and pit-patterned substrates are determined by atomic force microscopy (AFM)-based nanotomography. The observed differences in lateral and vertical composition gradients are correlated with the island morphology. This approach allowed us to employ AFM to simultaneously gather information on the composition and strain of SiGe islands. Our quantitative analysis demonstrates that for islands with a fixed aspect ratio, a modified geometry of the substrate provides an enhancement of the relaxation, finally leading to a reduced intermixing.

Keywords SiGe · Island · Alloying · Wet etching · Tomography · AFM · Lateral ordering

Introduction

The lattice mismatch between Si and Ge drives the formation of SiGe quantum dots (QD) during strained layer heteroepitaxy [1, 2]. For large-scale integration technologies [3], the position of such islands needs to be accurately controlled on the substrate surface [4]. A viable process relies on the fabrication of lithographically defined pits, which act as a sink for the deposited adatoms, allowing the exact positioning and addressability of individual QDs. In addition, a precise control of the chemical composition of the SiGe islands is required, since the three-dimensional (3D) composition profile ultimately determines their electronic behavior and optical properties. However, little work has been done on this topic, and the different intermixing mechanisms sustaining the growth and evolution of Ge islands in presence of a surface with an extrinsic morphology are still debated [5–7]. It has been shown that SiGe islands grown on patterned areas have larger volumes than those on the surrounding planar surfaces [8, 9]. These observations are corroborated by a recent comparison of X-ray measurements and finite element calculations, which suggests a different compositional state with a larger intermixing and relaxation on the patterned substrates [7]. However, the compositional differences at the single dot level were not yet considered.

In this letter we address the issue of the impact of substrate patterning on shape, composition, and strain relaxation at the single dot level by using atomic force microscopy (AFM)-based nanotomography (NT-AFM). Following Ref. [10], we have recently extended the capabilities of NT-AFM to quantitatively determine the full 3D composition profiles of strained SiGe islands [11]. In this study, we compare lateral and vertical composition gradients of individual SiGe islands grown on pit-pattern and planar Si(001) substrates. Above all, by combining structural data with the average island compositions as obtained by NT-AFM, we are able to determine island strain only by means of an AFM analysis. The experimental ability to

F. Pezzoli (✉) · M. Stoffel · A. Rastelli · O. G. Schmidt
Institute for Integrative Nanosciences, IFW Dresden,
Helmholtzstraße 20, 01069 Dresden, Germany
e-mail: f.pezzoli@ifw-dresden.de

A. Rastelli
e-mail: a.rastelli@ifw-dresden.de

Present Address:
M. Stoffel
Institut für Halbleitertechnik, Pfaffenwaldring 47,
70569 Stuttgart, Germany

T. Merdzhanova
Max-Planck-Institut für Festkörperforschung,
Heisenbergstraße 1, 70569 Stuttgart, Germany

map the chemical composition at the nanoscale helps indeed to shed new light on the driving forces governing alloying. Our findings provide direct experimental evidence that a nanostructured surface plays a major role in determining strain relaxation and therefore in defining the compositional profiles of the islands.

Experimental Procedure

The sample considered here consists of 8.5 monolayer of Ge deposited by molecular beam epitaxy at 700°C on a patterned Si(001) substrate [12]. A 500 × 500 μm^2 mesh of pits aligned along the ⟨110⟩ directions was realized by electron beam lithography followed by reactive ion etching. The distance between nearby pits is 450 nm and their depth and width about 25 and 85 nm, respectively. The surface morphology of the sample was analyzed by AFM operating in tapping mode with a super sharp silicon tip (nominal radius of curvature of 2 nm). Fig. 1a shows a 30 × 30 μm^2 AFM image of the surface morphology in proximity of a corner of the patterned area. The observed material depletion region is due to a directional diffusion of Ge from the unpatterned, flat surface toward the patterned area, which results in a gradient of the Ge amount available for island formation in the patterned area [9]. Islands close to the pattern edge are therefore larger than those a few microns away from it and some of them exceed the critical size for dislocation introduction [13]. Here we focus on the two areas marked in Fig. 1a, in order to exclude most of the large, dislocated islands at the boundaries of the patterned field. The two island ensembles consist mainly of barn-shaped islands [14], as corroborated by a facet analysis (not shown). As reported in Fig. 1b, the mean height of coherent islands is similar, being (49 ± 6) nm and (54 ± 3) nm on the flat and patterned surfaces, respectively. However, for a fixed island volume, V, the aspect ratio, r (defined as the ratio between height and the square root of the base area), turns out to be larger for islands grown on the flat surface, as shown in Fig. 1c. This result suggests some differences in the compositional and/or strain state. To study this further, we used a NT-AFM approach [11]. The sample was dipped in HF and then etched by means of an ammonium hydroxide–hydrogen peroxide solution (NHH),

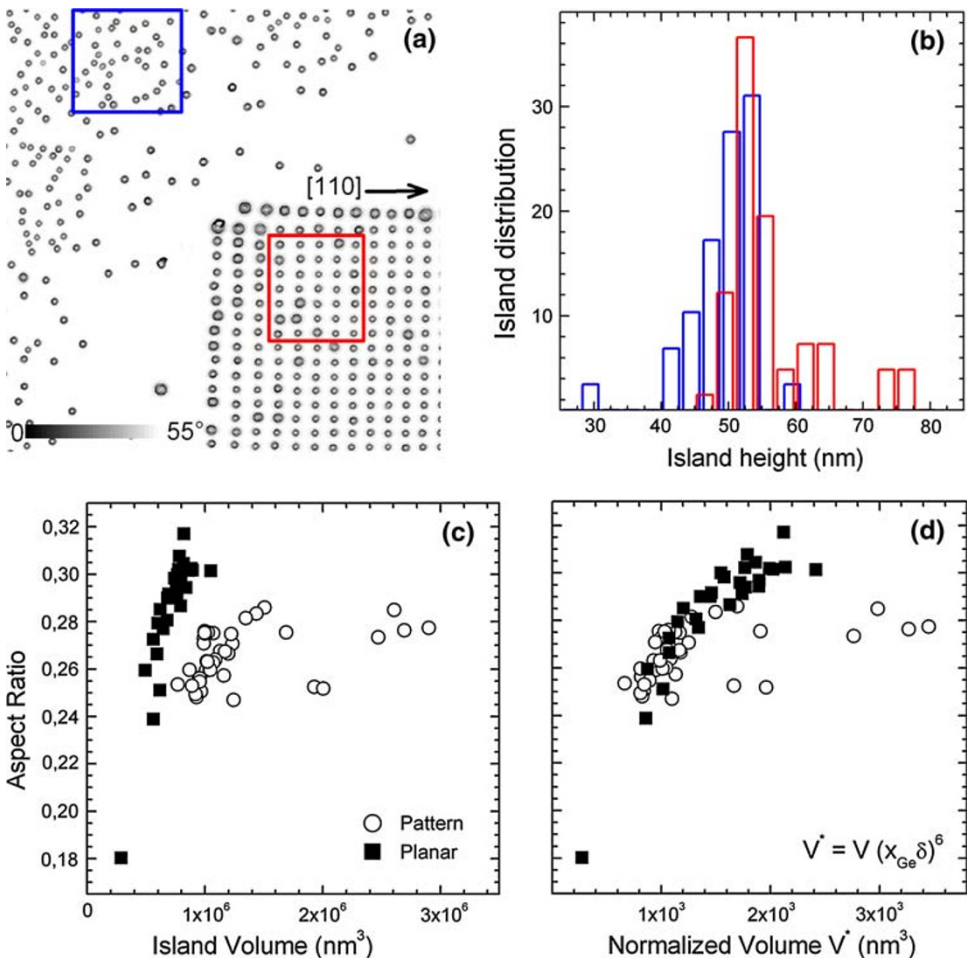

Fig. 1 (Color online) **a** 30 μm × 30 μm AFM scan of the sample surface close to a corner of the patterned area. The *gray* scale corresponds to the local surface slope with respect to the (001) plane. The analyzed areas on planar and patterned surface are marked in *blue* and *red*, respectively. **b** Height distribution of islands grown on pit-pattern (*red bars*) and flat surface (*blue*). **c**, **d** Island aspect ratio versus volume for islands in the regions marked in **a**. In **d** the island volumes have been rescaled according to x_{Ge}^6 and $(0.87 \times x_{Ge})^6$ for (*filled square*) and (*open circle*), respectively

with 1:1 vol. (28% NH_4OH):(31% H_2O_2). NHH is known to be rather insensitive to the strain over the whole composition range of SiGe alloys and to be isotropic, i.e., having no preferential etching direction [15]. Spatially resolved 3D contours of the Ge content, x_{Ge}, within the islands were obtained by measuring the same surface areas at increasing etching times [11]. The lateral and vertical resolution in the determination of x_{Ge} is given by the 3D matrix voxels, which have lateral and vertical side lengths of about 15 and 7 nm. The absolute uncertainty on x_{Ge} is about 0.02.

Results and Discussion

From the representative horizontal crosscuts of the stoichiometry profiles, shown in Fig. 2, it is observed that the Ge content within the islands is far from being uniform [11, 16–18]. Nevertheless, the lateral composition profiles of islands grown on pits tend to be more symmetric than for islands grown on the planar surface. The observed differences can be correlated with the lateral ordering. In the patterned field, as opposed to the random nucleation sites, the area from which individual islands collect adatoms during growth is almost equal, leading both to a regular dot arrangement and to an improved chemical homogeneity. The composition maps of islands grown on the flat surface (the left side of Fig. 2) show a decay of the Ge content from the apex to the base of the islands [16, 17]. This Ge accumulation at the island top is generally ascribed to chemical and elastic energy minimization [14, 19, 20]. The average Ge content at different height levels, z, above the substrate was then derived to highlight quantitative differences for the two island ensembles (see Fig. 3a). The Ge concentration both on flat and patterned substrate reveals a high chemical contrast at the base of the dot, reaching

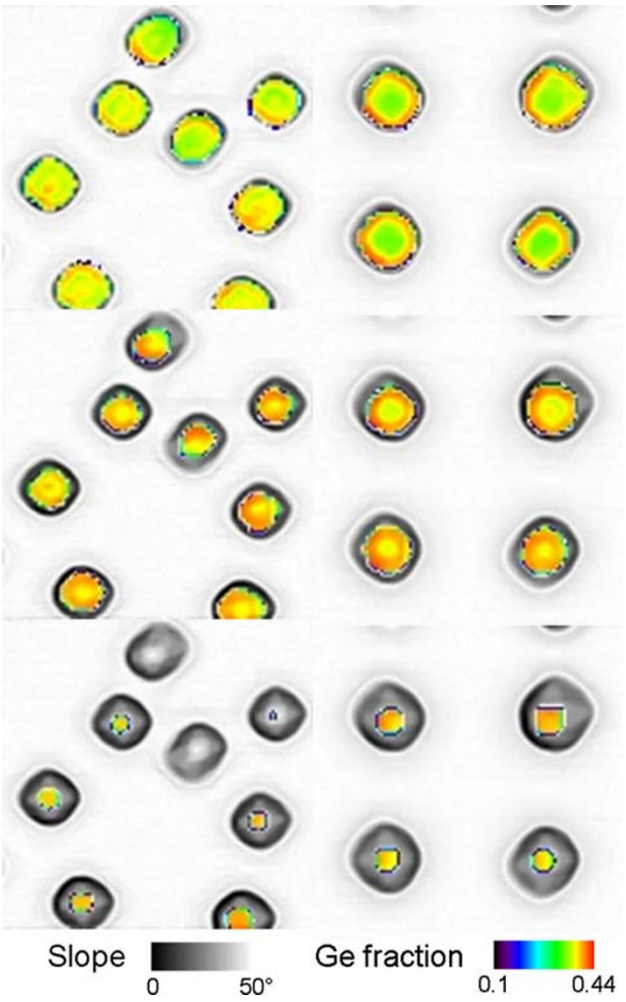

Fig. 2 (Color online) Sequence of 1 μm × 1 μm horizontal crosscuts at heights (*top* to *bottom* panels) z = 8, 22, and 39 nm, with respect to the Si substrate level, for islands on a flat (*left*) and patterned (*right*) surface area. The *gray* scale represents the local surface slope, while the Ge molar fraction is color coded

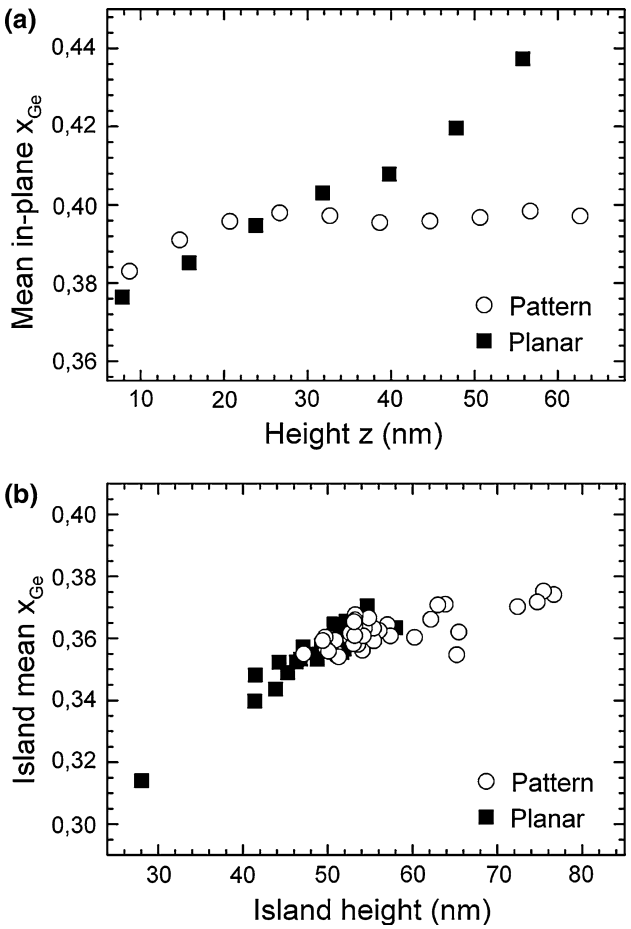

Fig. 3 **a** Average Ge content, x_{Ge}, for islands marked in Fig. 1**a**, as a function of z level with respect to the Si substrate (z = 0 nm). **b** Average Ge content of the islands as a function of their height. x_{Ge} error bars are of about 0.02

about $x_{Ge} = 0.38$ within the first 10 nm above the Si surface (see for a comparison Ref. [11] and references therein). Nevertheless, the data shown in Fig 3a point out that for $z \geq 10$ nm, the mean lateral Ge concentration increases monotonically for islands forming randomly on a flat surface, while it tends to a constant $x_{Ge} = 0.4$ for islands on the patterned substrate. This result provides an independent confirmation of those outlined in Ref. [7].

We focus now on the correlation between the morphological properties of the islands, i.e., island size and shape, and their average composition. The latter was evaluated by averaging the Ge content over all the matrix voxels of a given island. From Fig. 1c it is evident that the islands in the pits have a larger volume than those on flat substrates, which is in agreement with previous literature report, e.g., Ref. [8], whereas Fig. 4a shows that small islands are Si-richer than large islands. This is a general trend that does not depend on substrate geometry. It is worth noting that for a given volume, islands grown on pits have a slightly lower x_{Ge} as compared to islands grown on the flat surface (Fig. 4a). On the other hand, for a given island shape or aspect ratio value, $x_{Ge}^{pattern}$ is systematically larger than x_{Ge}^{planar}, as shown in Fig. 4b. Albeit counter intuitive, the results outlined above can be rationalized according to the following simple model concerning island relaxation. As follows from basic energy considerations, for coherent islands with fixed shape and homogeneous composition, the base length scales as the inverse square of the misfit, f [21, 22]. Therefore, the island volume V can be written as: $V(f) = V_0\ f^{-6}$, where V_0 is a constant which mainly depends on the shape of the island. For coherent islands, f is defined by the relative difference in the lattice parameters, ε, as: $f = \varepsilon \approx 0.04 x_{Ge}$. By using the average island values of x_{Ge} obtained from the NT-AFM analysis, volumes can be rescaled according to: $V^* = V(f)\ x_{Ge}^6$.

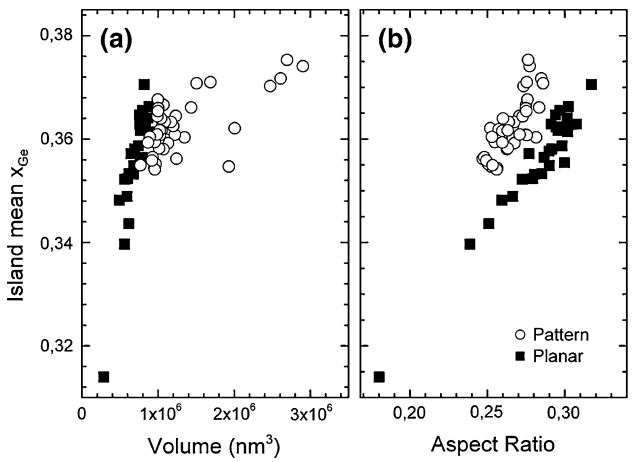

Fig. 4 Average Ge content of the islands as a function of their volume (**a**), and aspect ratio (**b**)

However, even with this rescaling, the two datasets of r vs. V^* do not overlap, which means that the different average composition is not able to explain why islands with similar volumes have different shapes, as reported in Fig. 1c. This discrepancy can be explained by the different relaxation of the two sets of islands. In fact, it is known that islands can relax strain energy more effectively in the pits, due to the surface curvature and valley filling [23, 24]. To estimate the enhanced strain relief, δ, the normalized island volumes on the patterned area can be written as: $V^*_{pit} = V^*\delta^6$. A good overlap of the two normalized volumes versus aspect ratio datasets is obtained, as shown in Fig. 1d, choosing $\delta \sim 0.87$. It can be therefore concluded that the strain in site-controlled islands is reduced by about 10% with respect to islands grown on the planar surface. According to this result, the strain, which is different for the two sets of islands, can be identified as the primary factor that determines the difference in the composition profiles. Pits indeed act as preferred nucleation locations for Ge adatoms, leading for a fixed aspect ratio to Ge-richer islands, as shown in Fig. 4b.

A possible, additional explanation for the aforementioned discrepancy is based on the different Ge profiles of the islands of the two ensembles as shown in Fig. 3a. Since the scaling law used in the present discussion is derived for island with a uniform composition, our simple approach holds more likely for islands grown on the pit-patterned surface, because of their more homogeneous Ge distribution (see Fig. 3a). Therefore, the δ value provided here has to be considered as an upper limit for the relaxation enhancement, since a realistic non-homogeneous Ge distribution for the coherent islands on the planar surface could lead to a more effective elastic energy reduction [20].

Nevertheless, some islands in Fig. 1d still do not follow the volume rescaling. According to their volumes, those islands are most probably plastically relaxed. In this case, the system lowers its total free energy by introducing dislocations. Therefore, the misfit in $V(f)$ has to be replaced by the residual misfit $f = \varepsilon - d$, where d is the plastic strain and the sign has been assigned according to the actual compressive stress.

Remarkably, the overall average Ge content is 0.361 ± 0.005 for islands grown on the pit-pattern and 0.36 ± 0.01 for islands on the flat surface area. As expected, despite an equal mean x_{Ge}, the standard deviation is a factor of two larger for the latter case, reflecting the larger composition fluctuations. Finally, the average Ge content of the individual islands increases monotonically with the island height (see Fig. 3b). This behavior can be rationalized as a result of the island evolution towards steeper and more relaxed morphologies. We can therefore compare islands with the same Ge content, e.g., about 0.36. These islands have the same height, i.e., about 55 nm

(Fig. 3b), but different aspect ratio (Fig. 4b). As a consequence, the island base and the volume are larger for islands grown on a pit-patterned surface. This can again be explained by the different residual strain of the two island ensembles.

Conclusions

In conclusion, an AFM-based nanotomography approach was used to gather in-depth information about the alloying and relaxation mechanism on both flat and pit-patterned substrates. The 3D compositional profiles reveal that islands forming on pit-patterned areas have a more uniform Ge distribution and are slightly Ge-richer than their counterparts forming on flat areas. These periodic Ge-rich island arrays are therefore appealing candidates for efficient local stress engineering in next generation Si field effect transistors [3] for ultra large-scale integration technologies.

Acknowledgements The authors acknowledge financial support by the EU D-DOTFET project (012150) and DFG (FOR 730).

References

1. D.J. Eaglesham, M. Cerullo, Phys. Rev. Lett. **64**, 1943 (1990)
2. J. Stangl, V. Holý, G. Bauer, Rev. Mod. Phys. **76**, 725 (2004)
3. O.G. Schmidt, K. Eberl, IEEE Trans. El. Dev. **48**, 1175 (2001)
4. O.G. Schmidt (ed.), *Lateral Alignment of Epitaxial Quantum Dots* (Springer, Berlin, 2007)
5. J.J. Zhang, M. Stoffel, A. Rastelli , O.G. Schmidt, V. Jovanović, L.K. Nanver, G. Bauer, Appl. Phys. Lett. **91**, 173115 (2007)
6. Z. Zhong , P. Chen, Z. Jiang, G. Bauer, Appl. Phys. Lett. **93**, 043106 (2008)
7. T.U. Schülli, G. Vastola, M.-I. Richard, A. Malachias, G. Renaud, F. Uhlík, F. Montalenti, G. Chen, L. Miglio, F. Schäffler, G. Bauer, Phys. Rev. Lett. **102**, 025502 (2009)
8. Z. Zhong, G. Bauer, Appl. Phys. Lett. **84**, 1922 (2004)
9. G.S. Kar, S. Kiravittaya, M. Stoffel, O.G. Schmidt, Phys. Rev. Lett. **93**, 246103 (2004)
10. R. Magerle, Phys. Rev. Lett. **85**, 2749 (2000)
11. A. Rastelli, M. Stoffel, A. Malachias, T. Merdzhanova, G. Katsaros, K. Kern, T.H. Metzger, O.G. Schmidt, Nano Lett. **8**, 1404 (2008)
12. M. Stoffel, A. Rastelli, T. Merdzhanova, G. Kar, O.G. Schmidt, Microelectron. J. **37**, 1528 (2006)
13. A. Marzegalli, V.A. Zinovyev, F. Montalenti, A. Rastelli, M. Stoffel, T. Merdzhanova, O.G. Schmidt , L. Miglio, Phys. Rev. Lett. **99**, 235505 (2007)
14. M. Stoffel, A. Rastelli, J. Tersoff, T. Merdzhanova, O.G. Schmidt, Phys. Rev. B **74**, 155326 (2006)
15. M. Stoffel, A. Malachias, T. Merdzhanova, F. Cavallo, G. Isella, D. Chrastina, H. von Känel, A. Rastelli, O.G. Schmidt, Semicond. Sci. Technol. **23**, 085021 (2008)
16. M. Floyd, Y. Zhang, K.P. Driver, J. Drucker, P.A. Crozier, D.J. Smith, Appl. Phys. Lett. **82**, 1473 (2003)
17. A. Malachias, S. Kycia, G. Medeiros-Ribeiro, R. Magalhães-Paniago, T.I. Kamins, R.S. Williams, Phys. Rev. Lett. **91**, 176101 (2003)
18. T.U. Schülli, M. Stoffel, A. Hesse, J. Stangl , R.T. Lechner, E. Wintersberger, M. Sztucki, T.H. Metzger, O.G. Schmidt, G. Bauer, Phys. Rev. B **71**, 035326 (2005)
19. N.V. Medhekar, V. Hegadekatte, V.B. Shenoy, Phys. Rev. Lett. **100**, 106104 (2008)
20. R. Gatti, F. Uhlík, F. Montalenti, New. J. Phys. **10**, 083039 (2008)
21. W. Dorsch, H.P. Strunk, H. Wawra, G. Wagner, J. Groenen, R. Carles , Appl. Phys. Lett. **72**, 179 (1998)
22. J.A. Floro, E. Chason , L.B. Freund, R.D. Twesten, R.Q. Hwang, G.A. Lucadamo, Phys. Rev. B **59**, 1990 (1999)
23. Z. Zhong, W. Schwinger, F. Schäffler, G. Bauer, G. Vastola, F. Montalenti, L. Miglio, Phys. Rev. Lett. **98**, 176102 (2007)
24. H. Hu, H.J. Gao, F. Liu, Phys. Rev. Lett. **101**, 216102 (2008)